IOPscience iopscience.iop.org

Home Search Collections Journals About Contact us My IOPscience

The elastic behaviour of natural single crystals of the high-spin compound MnS_2

This article has been downloaded from IOPscience. Please scroll down to see the full text article.

1990 J. Phys.: Condens. Matter 2 3713

(http://iopscience.iop.org/0953-8984/2/16/002)

View the table of contents for this issue, or go to the journal homepage for more

Download details:
IP Address: 171.66.16.103
The article was downloaded on 11/05/2010 at 05:53

Please note that terms and conditions apply.

J. Phys.: Condens. Matter **2** (1990) 3713–3721. Printed in the UK

The elastic behaviour of natural single crystals of the high-spin compound MnS_2

G A Saunders†, Wang Qingxian†, E F Lambson†, N Lodge†, D Paine† and W Hönle‡

† School of Physics, University of Bath, Claverton Down, Bath BA2 7AY, UK

‡ Max-Planck-Institut für Festkörperforschung, Heisenbergstrasse 1, 7000 Stuttgart 80, Federal Republic of Germany

Received 13 November 1989, in final form 12 January 1990

Abstract. The hydrostatic pressure and temperature dependences of velocities of ultrasonic modes propagated in natural single crystals of MnS_2 have been measured. The elastic stiffness tensor components C_{11} ($= 11.4 \pm 0.1) \times 10^{10}$ Pa), C_{12} ($= (3.0 \pm 0.2) \times 10^{10}$ Pa) and C_{44} ($= (3.6 \pm 0.1) \times 10^{10}$ Pa) and the bulk modulus B^S ($= (6.39 \pm 0.3) \times 10^{10}$ Pa) of this high-spin pyrite structure compound are much smaller than those of the low-spin isostructural crystal FeS_2. This is consistent with MnS_2 having substantially weaker attractive binding forces than those in FeS_2 as would be expected from its larger lattice parameter due in turn to the high-spin configuration of the manganese 3d electrons. The temperature dependences of the elastic stiffnesses measured between 4.2 K and 293 K show that the crystal softens elastically near the Néel temperature but other than this the elastic properties are very similar in the antiferromagnetic and paramagnetic phases. The hydrostatic pressure derivatives of the elastic stiffness tensor components $(\partial C_{11}/\partial P)_{P=0} = 8.9 \pm 0.1$, $(\partial C_{12}/\partial P)_{P=0} = 2.8 \pm 0.2$, $(\partial C_{44}/\partial P)_{P=0} = 3.9 \pm 0.1$ and $(\partial B^S/\partial P)_{P=0} = 4.79 \pm 0.3$ are all positive at room temperature: there is no acoustic mode softening under pressure. The results are used to describe the anharmonicity of the long wavelength acoustic modes in terms of mode Grüneisen parameters in the elastic continuum approximation. The mean long wavelength acoustic mode Grüneisen parameter γ^{el} ($= 2.4$) is much larger than the thermal Grüneisen parameter γ^{th} ($= 0.98$) which implies that the mode Grüneisen gammas for optic modes must on average be much smaller than those for the long wavelength acoustic phonons.

1. Introduction

The 3d transition metal chalcogenides MX_2 containing the dianion groups X_2^{2-} include compounds of major mineralogical importance and are interesting physically because of their wide range of electrical and magnetic properties. Four major structural types of these chalcogenides occur: pyrite (FeS_2), marcasite (FeS_2), arsenopyrite (FeAsS) and loellingite ($FeAs_2$). The details of chemical bonding and its relationship to energy band spectra in these related structures has been and remains a subject of wide interest (Brostigen and Kjekshus 1970, Kjekshus and Nicholson 1971, Goodenough 1972, Wilson 1972, Tossell *et al* 1981, Bullett 1982). The elastic properties can provide useful information about the nature and strength of the interatomic binding forces in crystals. Recently an ultrasonic study of FeS_2 was undertaken to resolve how its elastic behaviour varies with temperature and pressure (Benbattouche *et al* 1989). In spite of some previous indications to the contrary FeS_2 was shown to have a positive elastic stiffness

0953-8984/90/163713 + 09 $03.50 © 1990 IOP Publishing Ltd

tensor component C_{12}; hence its Poisson ratio takes the normal positive value; these quantities are not caused to become negative either by increase of pressure or change in temperature.

There are other fascinating problems associated with the elastic properties of MX_2 crystals. One of these concerns the relationship between elastic properties, lattice parameters and the 3d bonding states. While FeS_2 is a low spin compound, Mn^{2+} in MnS_2 is in the high spin state and has a magnetic moment corresponding to five unpaired electrons ($^6S_{5/2}$). As a result there is a substantial difference in the M–S bond length between these two isostructural compounds which can be expected to lead to considerable differences in their elastic behaviours. To find out if this is so, the elastic properties of manganese disulphide MnS_2 have now been measured.

High pressure x-ray diffraction experiments have shown that MnS_2 undergoes a pressure induced first order structural phase transition from the cubic pyrite to the orthorhombic marcasite phase at about 14 GPa (Chattopadhyay *et al* 1986). This is accompanied by a 15% volume change and has been associated with a transition from high spin to low spin of Mn^{2+}. There is a concomitant drastic increase in bulk modulus from that (76 GPa) in the pyrite phase to that (214 GPa) in the marcasite phase. The hydrostatic pressure dependences of each elastic stiffness tensor component C_{IJ} have now been determined individually. The results establish the vibrational anharmonicity of the long wavelength acoustic phonons for MnS_2.

The high spin configuration is observed for dichalcogenides of manganese; these compounds are antiferromagnetic semiconductors. Near 48 K MnS_2 undergoes a paramagnetic to antiferromagnetic transition (Hastings *et al* 1959, Westrum and Grønvold 1970, Lin and Hacker 1968, Hastings and Corliss 1976). This antiferromagnetic transition is first order (Hastings *et al* 1959, Lin and Hacker 1968, Chattopadhyay *et al* 1984). The antiferromagnetic ordering is of the third kind and involves unit cell doubling in the direction in which the magnetic moments alternate (Hastings *et al* 1959). The temperature dependences of the ultrasonic wave velocities, measured here from the boiling point of liquid helium to room temperature, have enabled the elastic properties to be determined in both the antiferromagnetic and paramagnetic phases of MnS_2 including the temperature range in the vicinity of the Néel point.

2. Experimental techniques

Natural single crystals of MnS_2 have been used for the investigations. They originated from Jeziorko in Poland and crystallised in the cube–octahedron morphology with well developed {1 0 0} and {1 1 1} faces. Before cutting and polishing the original edge lengths were approximately 8 mm. Chemical analyses were carried out using an inductively coupled plasma, ARL 35800 Quantoscan. The composition of the main constituents (not normalised) was found to be Mn: 45.40 wt% (calculated 46.14 wt%) and S: 52.60 wt% (calculated 53.86 wt%), yielding a Mn : S ratio equivalent to $MnS_{1.99(2)}$. The following trace elements were found to be present (wt%): P = 0.03, As = 0.02, Al = 0.04, Zn = 0.13, Fe = 0.10, Ni = 0.02, Na = 0.06, Ca = 0.01, In = 0.13, Si = 1.08, O = 0.66 (not normalised to 100%).

The crystals were also examined by x-ray powder diffraction. The compound consists of Mn^{2+} and an S_2^{2-} molecular anion. The cubic pyrite structure (C2, paramagnetic space group Pa3) has a NaCl-like arrangement of the Mn^{2+} ions and the centre of the S_2^{2-} group. The structure is primitive cubic since the axes of the four X_2 groups in the unit

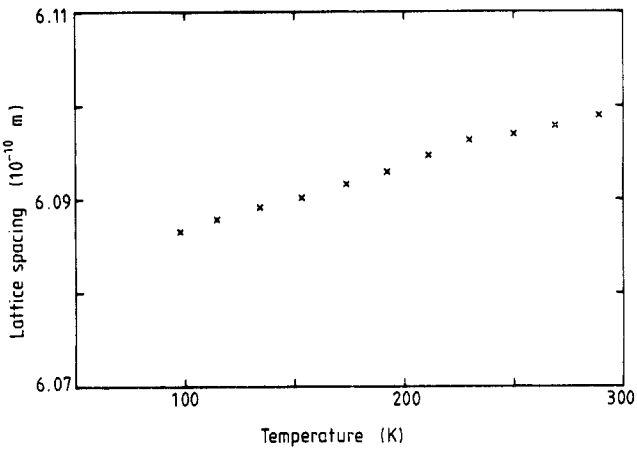

Figure 1. The temperature dependence of the lattice parameter a_0 of MnS_2.

cell are parallel to different body diagonals. The lattice parameter a_0 was found to be almost linearly dependent upon temperature between 100 K and 290 K (figure 1). These results correspond to a mean linear coefficient α of thermal expansion over this range of temperature of $(1.04 \pm 0.1) \times 10^{-5}\ K^{-1}$. That of FeS_2 estimated (Benbattouche *et al* 1989) from the lattice parameter data of Bindloss (1971) is $0.85 \times 10^{-5}\ K^{-1}$.

The velocities for 10 MHz ultrasound modes propagated in the [100], [111] and [110] directions were measured by the pulse echo overlap technique. Results were corrected for transducer diffraction effects by the methods developed by Kittinger (1977). The elastic stiffness tensor components at room temperature (293 K) determined as the statistical means of many mode velocity measurements are compared in table 1(*a*) with those of FeS_2 at 295 K. The temperature dependences of ultrasonic wave velocities were measured in a liquid helium cryostat, the sample temperatures being determined using a gold–iron–chromel thermocouple. The experimental results are plotted in figure 2.

The effect of pressure on ultrasonic mode velocities at room temperature was determined using the experimental techniques employed previously for FeS_2 (Benbattouche *et al* 1989). The 'natural' velocity (Thurston and Brugger 1964) of each ultrasonic mode was linearly dependent upon pressure up to the highest pressure (2.0×10^8 Pa) applied. The hydrostatic pressure derivatives $(\partial C_{IJ}/\partial P)_{P=0}$ have been determined from these pressure measurements and are given in table 1.

3. Discussion

In the pyrite structure the distorted octahedral crystal symmetry splits the cation d band into two sections: the bonding t_{2g}, which can contain six electrons, and the higher energy, antibonding e_g which can hold four. The Fermi energy is close to the d band and its relationship across the series of transition metal dichalcogenides MX_2 to antibonding and bonding states as the number of 3d electrons changes, leads to the wide range of properties observed for these compounds. There is a pronounced effect of the t_{2g} versus e_g occupation on the lattice parameter and the M–X bond length for the high spin and low spin divalent transition metal chalcogenides. This is graphically illustrated in figure 10 of Wilson (1972); comparison of the M–S distances with those of other 3d

Table 1 (*a*) The elastic properties of MnS_2 at room temperature (293 K) in comparison with those of FeS_2 (Benbattouche *et al* 1989). (*b*) Directional components of Young's modulus and Poisson's ratio for MnS_2 at 293 K.

(*a*)	MnS_2	FeS_2
Lattice parameter a_0 (10^{-10} m)	6.098 ± 0.02	5.418
Density (kg m^{-3})	3502	5016
Elastic stiffness (10^{10} Pa)		
C_{11}	11.4 ± 0.1	36.6 ± 0.02
C_{12}	3.0 ± 0.2	4.9 ± 0.1
C_{44}	3.6 ± 0.1	10.3 ± 0.1
$C' = (C_{11} - C_{12})/2$	3.05 ± 0.05	15.9 ± 0.1
Bulk modulus B_0^S (10^{10} Pa)	6.39 ± 0.3	15.5 ± 0.2
Elastic compliance (10^{-10} Pa^{-1})		
S_{11}	0.109	0.028
S_{12}	−0.028	−0.003
S_{44}	0.276	0.097
Volume compressibility (10^{-10} Pa^{-1})	0.171	0.064 ± 0.002
Hydrostatic pressure derivatives		
$(\partial C_{11}/\partial P)_{P=0}$	8.9 ± 0.1	13.3 ± 0.1
$(\partial C_{12}/\partial P)_{P=0}$	2.8 ± 0.2	4.1 ± 0.2
$(\partial C_{44}/\partial P)_{P=0}$	3.9 ± 0.1	1.7 ± 0.1
$(\partial C'/\partial P)_{P=0}$	3.05 ± 0.08	4.6 ± 0.1
$(\partial B^S/\partial P)_{P=0}$	4.79 ± 0.3	7.2 ± 0.1
Thermodynamic pressure derivatives		
B_{11}	10.5	15.1
B_{12}	1.9	3.21
B_{44}	5.1	2.93
TOEC combinations (10^{11} Pa)		
$C_{111} + 2C_{112}$	−183	−70.4
$C_{144} + 2C_{166}$	−89	−13.6
$C_{123} + 2C_{112}$	−34	−14.9
Mean long-wavelength acoustic mode Grüneisen parameter γ^{el}	2.4	1.83
Thermal Grüneisen parameter γ^{th}	0.98	1.54

(*b*) Young's modulus (10^{10} Pa)			
$E_{[001]}$		10.1 ± 0.1	
$E_{[110]}$		9.3 ± 0.1	
$E_{[111]}$		9.0 ± 0.1	
Poisson's ratio:	Stress direction	Strain direction	
σ_1	[001]	In (001) plane	0.212 ± 0.002
σ_2	[110]	[011]	0.194 ± 0.003
σ_3	[110]	[110]	0.276 ± 0.002
σ_4	[111]	In (111) plane	0.242 ± 0.003

transition metal disulphides MS_2 (M = Fe, Co, Ni, Cu and Zn) shows that for MnS_2 the Mn–S distance is well above the plot as a function of the d^i configuration found for the other compounds. The manganese ion in MnS_2 is in the high spin, half-filled d^5 shell configuration ($t_{2g}^3 e_g^2$); the room temperature lattice parameter (6.106 Å) and the Mn–S distance (2.59 Å) are large compared with those in FeS_2 which contains low spin Fe^{2+} (t_{2g}^6) and has the smaller lattice parameter of 5.418 Å (the Fe–S distance is 2.26 Å).

Comparison between the elastic stiffness tensor components of MnS_2 and FeS_2 at room temperature (table 1) shows that elastically FeS_2 is much the stiffer crystal. C_{11} is more than three times larger for FeS_2 than for MnS_2. The bulk moduli of these two

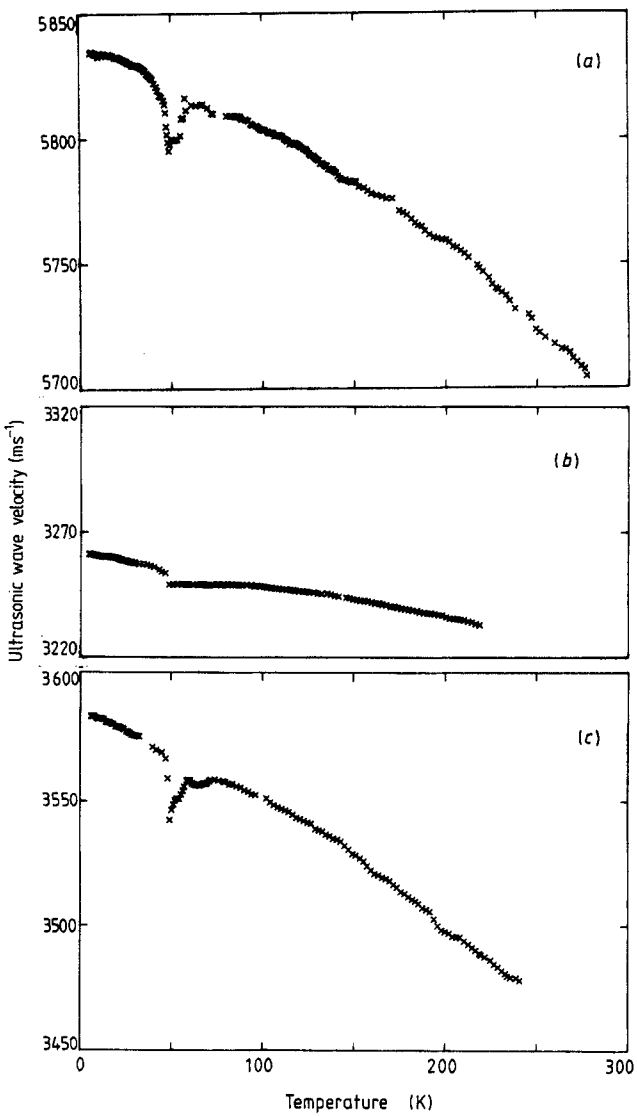

Figure 2. Temperature dependences of the velocity of ultrasonic waves propagated in MnS_2: (*a*) the longitudinal mode along the [001] direction; (*b*) the shear mode along the [001] direction; (*c*) the shear mode along the [1 1 0] direction.

isostructural compounds are in the ratio of 2.4 : 1. MnS_2 is much easier to compress than FeS_2, a feature attributed by Chattopadhyay and von Schnering (1985) to its high spin, large M–S distance state. The complexity of the energy band structures of these transition metal pyrite structure compounds preclude a model calculation here of the elastic stiffness tensor compounds or even the bulk modulus. However, a qualitative appreciation of the effect of the difference in lattice parameters between MnS_2 and FeS_2 on the attractive contribution to the interatomic binding forces can be obtained by a comparison on the basis of the simplistic ionic model of the Madelung constants (α_M) and energies; FeS_2: $a_0 = 5.4181$ Å, $\alpha_M = 3.2292$, attractive energy 1985 kJ mol^{-1}; MnS_2: $a_0 = 6.106$ Å, $\alpha_M = 2.6238$, attractive energy 1743 kJ mol^{-1}. Of course for these mixed covalent–ionic

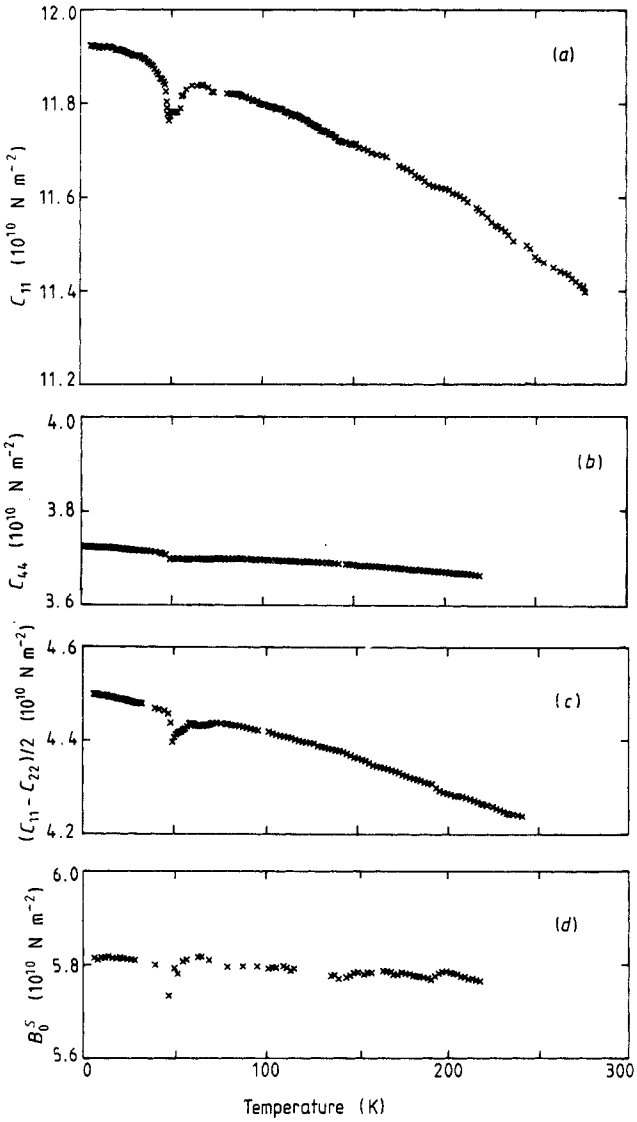

Figure 3. Temperature dependences of (*a*) C_{11}, (*b*) C_{44}, (*c*) $(C_{11} - C_{12})/2$ and (*d*) the adiabatic bulk modulus B_0^S of MnS_2.

compounds a Madelung model suffers from its neglect of non-central, non-ionic forces and so its predictions have no quantitative validity.

The temperature dependences of the elastic stiffness constants (figure 3) show that C_{11} and $(C_{11} - C_{12})/2$ (corresponding to a shear in a $[1\bar{1}0]$ direction on a (110) plane) soften as the crystal is cooled down through the Néel temperature (48 K). In the absence of any measurement of the thermal expansion of MnS_2 in the vicinity of T_N, it is not possible to separate the influence of dimensional changes due to magnetostriction from ΔE or magnetoelastic contributions. Below T_N the elastic stiffnesses and the bulk modulus recover and are closely similar in both the antiferromagnetic and paramagnetic

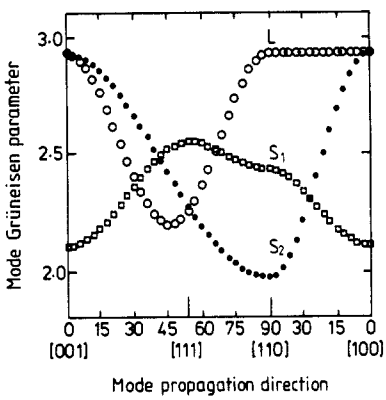

Figure 4. The acoustic mode Grüneisen parameter in the long wavelength limit for modes in the quasi-longitudinal (L) and quasi-shear (S_1 and S_2) branches as a function of the propagation direction in MnS_2.

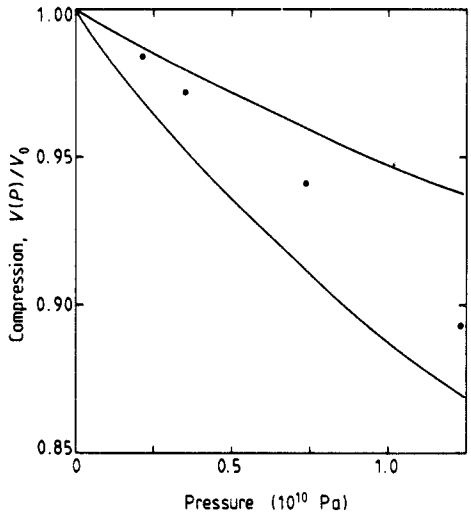

Figure 5. The compressions $V(P)/V_0$ for MnS_2 and FeS_2 obtained by using the Murnaghan (1944) equation of state (2) using the isothermal bulk modulus B_0^T and its hydrostatic pressure derivative measured ultrasonically. The lower curve corresponds to the compression of MnS_2 while the upper one is for FeS_2. The filled circles correspond to the compression of MnS_2 measured in a diamond anvil pressure cell by Chattopadhyay and von Schnering (1985).

phases. To find the total differences between the elastic stiffnesses in the paramagnetic and antiferromagnetic phases, the data in figure 3 in the paramagnetic phase have been extrapolated below T_N. The changes incurred in the C_{IJ} when the crystal has become antiferromagnetic are small ($\Delta C_{44}/C_{44} = 0.7\% \pm 0.1\%$; $\Delta C_{11}/C_{11} = 0.6\% \pm 0.1\%$; $\Delta C'/C' = 0.6\% \pm 0.1\%$): it is not possible to separate readily the magnetic contributions to the elastic energy from sources such as ΔE, the magnetoelastic and the magnetostrictive effects. The magnetic structure below the transition temperature T_N is a type III antiferromagnet. The transition is described by an $n = 6$ Landau–Ginsburg–Wilson Hamiltonian, which is an extensive universality class of magnetic systems (Bak and Mukamel 1976). Although it would be of considerable interest to test the universality by examining the ultrasonic velocity or attenuation dependence upon temperature near T_N, this has not proved possible for these natural single crystals whose perfection is not good enough to obtain data of the high sensitivity and accuracy required for this purpose.

The positive signs found for the hydrostatic pressure derivatives $(\partial C_{IJ}/\partial P)_{P=0}$ of the elastic stiffness tensor components (table 1) show that for MnS_2 the long wavelength acoustic mode frequencies increase under pressure in the normal way. This is also so for FeS_2 (Benbattouche *et al* 1989). These data quantify (to the cubic term in the Hamiltonian with respect to Lagrangian strain) the vibrational anharmonicity of these modes. The acoustic mode Grüneisen parameters, determined computationally from the components of the elastic stiffness tensor and their pressure derivatives given in table 1(*a*) using the method of Brugger and Fritz (1967), are plotted in figure 4 as a function of the propagation direction in the symmetry planes. The modes labelled L correspond to those close to the Brillouin zone centre for the longitudinal acoustic branch and those labelled S_1 and S_2 to the two shear branches. Only modes propagated along the symmetry

directions are pure longitudinal or shear in type; the polarisation and propagation vectors are not mutually orthogonal for the other acoustic modes which are in consequence usually described as being either quasi-longitudinal or quasi-shear. All the long wavelength acoustic modes stiffen under pressure which causes an increase in mode frequency (or energy) in the normal way expected for a crystal in which there is no tendency towards instability. A mean long wavelength acoustic mode Grüneisen parameter γ^{el} (table 1) has been calculated as

$$\tfrac{1}{3}\sum_p \int \gamma(p, N)\, d\Omega/4\pi.$$

The non-linear acoustic behaviour, expressed by this mean elastic Grüneisen parameter γ^{el}, can be used in combination with specific heat C_p (Westrum and Grønvold 1970), thermal expansion and bulk modulus B^S data to obtain an overall insight into the vibrational anharmonicity of MnS_2. The thermal Grüneisen parameter

$$\gamma^{th} = 3\alpha V B^S / C_p = \sum_i \gamma_i C_i \Big/ \sum_i C_i \tag{1}$$

sums over the mode Grüneisen gammas γ_i for the states excited at a given temperature, C_i being the Einstein specific heat for mode i. The finding that the value 0.98 of γ^{th} at room temperature (292 K) is much smaller than γ^{el} (= 2.4) implies that the mode Grüneisen gammas for optic modes and acoustic modes for wavevectors away from $\boldsymbol{k} = 0$ must on average be much smaller than those for the long wavelength acoustic phonons. This feature of MnS_2 is probably a consequence of its structure and interatomic binding forces, and in particular of the presence of S_2^{2-} molecular anions. The intramolecular volume should be much less compressible than interionic volume: Grüneisen gammas of those optic modes associated with internal vibrations of the strongly bound S_2^{2-} molecular anion can be expected to be close to zero so their contribution should reduce the value of γ^{th}. As the temperature is decreased the thermal Grüneisen parameter γ^{th} increases becoming 1.6 at 100 K (the lower limit of the data obtained for thermal expansion). This is due to the increase in the relative proportion of the low energy, long wavelength, acoustic phonons with the large mean γ^{el} as the higher energy phonons, especially those in the states of higher energy corresponding to internal vibrations of the S_2^{2-} anions, are frozen out with decreasing temperature. The thermal Grüneisen parameter of MnS_2, γ^{th} (= 0.98), is substantially smaller than that (1.54) of FeS_2 (Benbattouche *et al* 1989). This difference in vibrational anharmonicity between the two compounds is attributable to the difference in lattice parameters and hence to the weaker interatomic binding forces in the high spin compound MnS_2 compared to those in low spin FeS_2.

Another property that is sensitive to the strength of interionic binding forces is the compression $V(P)/V_0$ (the ratio of the volume $V(P)$ at a pressure P to that V_0 at atmospheric pressure). This has been estimated (figure 5) for MnS_2 and FeS_2 using the Murnaghan (1944) equation of state written in logarithmic form as

$$\ln\left(\frac{V_0}{V(P)}\right) = \frac{1}{B_0'^T} \ln\left[B_0'^T\left(\frac{P}{B_0^T}\right) + 1\right] \tag{2}$$

The isothermal bulk modulus B_0^T and its hydrostatic pressure derivative $B_0'^T$ used for FeS_2 are 1.549×10^{11} Pa and 7.14 respectively (Benbattouche *et al* 1989). For MnS_2 these quantities, derived from the adiabatic quantities B_0^S and $B_0'^S$ (table 1) using thermodynamic relationships listed by Yogurtçu *et al* (1985), are 6.33×10^{10} Pa and 4.71

respectively. Chattopadhyay and von Schnering (1985) obtained B_0^T as 7.60×10^{10} Pa and $B_0'^T$ as 5.4 from measurements of the dependence of the lattice parameters upon high pressure in a diamond anvil cell. The compression $V(P)/V_0$ determined from the ultrasonic data is in reasonable agreement with the values for MnS_2 in its pyrite form obtained from the diamond anvil cell experiments (figure 5). The compression of the pyrite structure form of MnS_2 is much greater than that of the more strongly bound iron pyrite FeS_2. At about 1.40×10^{10} Pa MnS_2 undergoes a pressure induced transformation involving a 15% volume contraction from the high spin pyrite to the low spin marcasite-type phase (Chattopadhyay and von Schnering 1985). In the high pressure phase MnS_2 has an isothermal bulk modulus of 2.14×10^{11} Pa, so that it has a compressibility comparable to that of FeS_2 for which Chattopadhyay and von Schnering (1985) determined B_0^T as 2.15×10^{11} Pa by the same experimental high pressure technique. That comprised an important step towards the conclusion that the linear and non-linear acoustic properties of MnS_2 and FeS_2 differ substantially due to the difference between their M–S bond lengths which arises from the high spin and low spin configurations of the transition metal ion.

Acknowledgment

We are grateful to Mrs O Buresch of the Max-Planck-Institut für Festkörperforschung for the inductively coupled plasma sample analysis.

References

Bak P and Mukamel D 1976 *Phys. Rev.* B **13** 5086–94
Benbattouche N, Saunders G A, Lambson E F and Hönle W 1989 *J. Phys. D: Appl. Phys.* **22** 670–5
Bindloss W 1971 *J. Appl. Phys.* **42** 1474–5
Brostigen G and Kjekshus A 1970 *Acta Chem. Scand.* **24** 2993–3012
Brugger K and Fritz T C 1967 *Phys. Rev.* **157** 524–31
Bullett D W 1982 *J. Phys. C: Solid State Phys.* **15** 6163–74
Chattopadhyay T and von Schnering H G 1985 *J. Phys. Chem. Solids* **46** 113–6
Chattopadhyay T, von Schnering H G and Graf H A 1984 *Solid State Commun.* **50** 865–7
Chattopadhyay T, von Schnering H G and Grosshans W A 1986 *Physica* B **139 + 140** 305–7
Goodenough J B 1972 *J. Solid State Chem.* **5** 144–52
Hastings J M and Corliss L M 1976 *Phys. Rev.* B **14** 1995–6
Hastings J M, Elliott N and Corliss L M 1959 *Phys. Rev.* **115** 13–7
Kittinger E 1977 *Ultrasonics* **15** 30–2
Kjekshus A and Nicholson D G 1971 *Acta Chem. Scand.* **25** 866–76
Lin M S and Hacker H 1968 *Solid State Commun.* **6** 687–9
Murnaghan F D 1944 *Proc. Natl Acad. Sci. USA* **30** 244–7
Thurston R N and Brugger K 1964 *Phys. Rev.* **133** A1604–10
Tossell J A, Vaughan D J and Burdett J K 1981 *Phys. Chem. Mineral.* **7** 177–84
Westrum E F and Grønvold F 1970 *J. Chem. Phys.* **52** 3820–6
Wilson J A 1972 *Adv. Phys.* **21** 143–98
Yogurtçu Y K, Saunders G A and Riedi P C 1985 *Phil. Mag.* A **52** 833–46